

## Improving the Thermodynamic Energy Efficiency of Battery Electrode Deionization Using Flow-Through Electrodes

Moon Son, Vineeth Pothanamkandath, Wulin Yang, Johannes Vrouwenvelder, Christopher A. Gorski, and Bruce E. Logan

*Environ. Sci. Technol.*, **Just Accepted Manuscript** • DOI: 10.1021/acs.est.9b06843 • Publication Date (Web): 24 Feb 2020

Downloaded from pubs.acs.org on February 27, 2020

### Just Accepted

“Just Accepted” manuscripts have been peer-reviewed and accepted for publication. They are posted online prior to technical editing, formatting for publication and author proofing. The American Chemical Society provides “Just Accepted” as a service to the research community to expedite the dissemination of scientific material as soon as possible after acceptance. “Just Accepted” manuscripts appear in full in PDF format accompanied by an HTML abstract. “Just Accepted” manuscripts have been fully peer reviewed, but should not be considered the official version of record. They are citable by the Digital Object Identifier (DOI®). “Just Accepted” is an optional service offered to authors. Therefore, the “Just Accepted” Web site may not include all articles that will be published in the journal. After a manuscript is technically edited and formatted, it will be removed from the “Just Accepted” Web site and published as an ASAP article. Note that technical editing may introduce minor changes to the manuscript text and/or graphics which could affect content, and all legal disclaimers and ethical guidelines that apply to the journal pertain. ACS cannot be held responsible for errors or consequences arising from the use of information contained in these “Just Accepted” manuscripts.

1 Date: January 28, 2020  
2 Revision submitted to: *Environmental Science & Technology*

3  
4 **Improving the Thermodynamic Energy Efficiency of Battery Electrode**  
5 **Deionization Using Flow-Through Electrodes**

6 Moon Son <sup>a</sup>, Vineeth Pothanamkandathil <sup>a</sup>, Wulin Yang <sup>a</sup>, Johannes S. Vrouwenvelder <sup>b</sup>,  
7 Christopher A. Gorski <sup>a</sup>, Bruce E. Logan <sup>a,\*</sup>

8 <sup>a</sup> Department of Civil and Environmental Engineering, The Pennsylvania State  
9 University, University Park, PA 16802, USA

10 <sup>b</sup> Water Desalination and Reuse Center (WDRC), Division of Biological and  
11 Environmental Science and Engineering (BESE), King Abdullah University of Science  
12 and Technology (KAUST), Thuwal 23955-6900, Saudi Arabia

13 \* Corresponding author. Email: [blogan@psu.edu](mailto:blogan@psu.edu); Tel.: +1-814-863-7908  
14

15 **Abstract**

16 Ion intercalation electrodes are being investigated for use in mixed capacitive deionization (CDI)  
17 and battery electrode deionization (BDI) systems because they can achieve selective ion removal  
18 and low energy deionization. To improve the thermodynamic energy efficiency (*TEE*) of these  
19 systems, flow-through electrodes were developed by coating porous carbon felt electrodes with a  
20 copper hexacyanoferrate composite mixture. The *TEE* for ion separation using flow-through  
21 electrodes was compared to a system using flow-by electrodes with the same materials. The  
22 flow-through BDI system increased the recoverable energy nearly threefold (0.009 kWh m<sup>-3</sup>,  
23 compared to a 0.003 kWh m<sup>-3</sup>), which increased the *TEE* from ~6% to 8% (NaCl concentration  
24 reduction from 50 mM to 42 mM; 10 A m<sup>-2</sup>, 50% water recovery, and 0.5 mL min<sup>-1</sup>). The *TEE*  
25 was further increased to 12% by decreasing the flow rate from 0.50 mL min<sup>-1</sup> to 0.25 mL min<sup>-1</sup>.  
26 These findings suggest that under similar operational conditions and materials, flow-through  
27 battery electrodes could achieve better energy recovery and *TEE* for desalination than flow-by  
28 electrodes.

## 29 Introduction

30 Several different electrochemical processes, including capacitive deionization (CDI),  
31 electrodialysis, shock electrodialysis, and electro-forward osmosis, are being investigated as  
32 methods to achieve more efficient deionization of brackish waters.<sup>1-8</sup> CDI has been widely  
33 investigated due to its use of inexpensive electrode materials, such as activated carbon, and  
34 relatively low energy requirements ( $<0.5 \text{ kWh m}^{-3}$  for  $<25 \text{ mM NaCl}$ ).<sup>9-15</sup> A typical CDI cell  
35 consists of two capacitive electrodes that remove ions via an electrostatic double layer when  
36 current is applied. The ions held by the electrodes in the first charging step are released in a  
37 second discharging step by alternating the direction of the applied current. One disadvantage of  
38 CDI is that high applied voltages ( $>1.2 \text{ V}$ ) can result in parasitic Faradaic reactions, such as  
39 hydrogen evolution at the cathode or anode oxidation.<sup>16, 17</sup>

40 A slightly different approach to electrochemical desalination is based on one or both of the  
41 capacitive electrodes being replaced by battery-type or intercalation materials such, as Prussian  
42 Blue or manganese oxides.<sup>18-21</sup> This process, called Faradaic deionization,<sup>22</sup> cation intercalation  
43 desalination,<sup>23</sup> or battery electrode deionization (BDI),<sup>19, 24</sup> can reduce the energy used for  
44 desalination compared to CDI as specific voltages are used to intercalate the ions into the  
45 electrode material, rather than hold them on the electrode surface. In recent BDI tests using the  
46 Prussian Blue analogue copper hexacyanoferrate (CuHCF),<sup>19</sup> efficient desalination was achieved  
47 at an applied voltage of  $0.6 \text{ V}$ , with  $0.02 \text{ kWh m}^{-3}$  for a triple stack of ion exchange membranes,  
48 and  $0.05 \text{ kWh m}^{-3}$  for a single membrane ( $25 \text{ mM NaCl}$  influent and  $17 \text{ mM}$  effluent). In  
49 contrast,  $\sim 0.2 \text{ kWh m}^{-3}$  was required using CDI under the same experimental conditions.<sup>19</sup> One  
50 goal for improving the efficiency of the BDI process is to increase the thermodynamic energy  
51 efficiency (*TEE*) of the system, where *TEE* is defined as the amount of energy used by an actual  
52 system relative to the thermodynamic minimum energy required to achieve a particular salt

53 separation.<sup>25</sup>

54 To improve the overall efficiency of the BDI system, we examined the use of flow-through  
55 electrodes constructed by depositing a composite mixture of CuHCF, binder, and carbon black  
56 into a highly porous graphite felt substrate. The complete cell consisted of two flow-through  
57 CuHCF electrodes in direct contact with an anion exchange membrane (AEM) placed in the  
58 middle of the chamber. This configuration is slightly different from a flow-through CDI process,  
59 where an AEM is not usually used, and where the feed stream flows perpendicular to the  
60 electrodes.<sup>26</sup> In the flow-through BDI system, the feed stream penetrates the electrode in a  
61 direction parallel to the water flow. Sodium ions are intercalated into the positive electrode while  
62 chloride ions migrate through the AEM towards the counter electrode. A semi-continuous  
63 treatment process is created by switching the direction of the applied voltage (0.6 V). While  
64 there have been several flow-through CDI systems,<sup>27-30</sup> there is only one previously reported  
65 flow-through electrode system which used a serpentine construction for channeling flow through  
66 the electrode in BDI.<sup>23</sup> In addition, that study did not provide comparisons with flow-by  
67 electrodes with the same architecture. Thus, one of the objectives of this study was to compare  
68 *TEE* values recorded for BDI systems using flow-through or flow-by electrodes with the same  
69 general architecture. In typical CDI systems that use porous carbon electrodes, a higher average  
70 salt adsorption rate was observed in the flow-through mode compared to the flow-by mode due  
71 to the longer electrode-solution contact time.<sup>26, 31</sup> However, this increased adsorption rate results  
72 in a decreased *TEE* in the flow-through mode due to the additional resistance of the separator in  
73 between two electrodes and increased rates of faradaic side reactions.<sup>13, 32, 33</sup> Unlike a CDI  
74 system, the BDI system does not have a separator in the water path, and it operates at relatively  
75 low voltage, which could increase *TEE* values. To more fully evaluate the impact of the flow-

76 through configuration, we compared flow-through BDI electrodes with a flow-by configuration  
77 used in our previous studies.<sup>19</sup> To further improve performance, the flow-through configuration  
78 was also examined with higher CuHCF loading. The performance of these systems was  
79 evaluated in terms of specific adsorption capacity of Na<sup>+</sup> ions, specific capacity of charge, charge  
80 efficiency, cycling efficiency, energy consumption, energy recovery, and *TEE*.

81

## 82 **Materials and methods**

83 **Battery Electrode Fabrication.** CuHCF powder was synthesized using a co-precipitation  
84 method as previously reported.<sup>19, 24</sup> Briefly, the same amounts of 0.1 M Cu(NO<sub>3</sub>)<sub>2</sub> (Sigma-  
85 Aldrich) and 0.05 M K<sub>3</sub>[Fe(CN)<sub>6</sub>] (J.T.Baker) were added to deionized (DI) water with vigorous  
86 stirring. The precipitates were washed by centrifugation and dried overnight in a vacuum oven to  
87 produce the CuHCF powder. A slurry of CuHCF (80 wt%), carbon black (10 wt%, Vulcan  
88 XC72R, Cabot, average particle size: 50 nm), and polyvinylidene fluoride (10 wt%, Kynar HSV  
89 900, Arkema Inc) in 1-methyl-2-pyrrolidinone (Sigma-Aldrich) was loaded onto the substrate  
90 using a pipette to fabricate electrodes containing 5 mg cm<sup>-2</sup> of the slurry (4 mg cm<sup>-2</sup> of CuHCF).  
91 A graphite felt substrate (3.0 mm thick and ~31 mg cm<sup>-2</sup>; CeTech, GF030) was used to make the  
92 flow-through (FT) electrodes, while carbon cloth (0.25 mm thick and ~20 mg cm<sup>-2</sup>; AvCarb  
93 Material Solutions, 1071 HCB) was used for the control experiments with flow-by (FB)  
94 electrodes. Preliminary tests showed that it was possible approximately double the amount of  
95 CuHCF slurry added to the felt electrodes; further addition of the slurry clogged the electrode so  
96 that no flow could be passed through the electrode. For the double-loaded electrodes, 10 mg  
97 cm<sup>-2</sup> of the slurry containing 8 mg cm<sup>-2</sup> of CuHCF was loaded onto carbon cloth (FB-D) or  
98 graphite felt substrates (FT-D). All the electrodes were heated and dried at 70°C using a vacuum

99 oven to remove the solvent.

100 **Electrode Characterization.** Scanning electron microscopy (SEM, Apreo, ThermoFisher  
101 Scientific) and energy dispersive X-ray spectroscopy (EDS) were used to determine the  
102 morphology and dispersion of CuHCF powder in the electrodes. Standard and backscatter  
103 detectors were used to ensure a distinction between CuHCF powder and carbon-based substrates.  
104 No separate conductive coating of the samples was conducted since the electrode itself was  
105 highly conductive.

106 The electrode porosity ( $P$ , %), was calculated using<sup>34</sup>

$$P = \frac{W_w - W_d}{E_a h} \times 100 \quad (1)$$

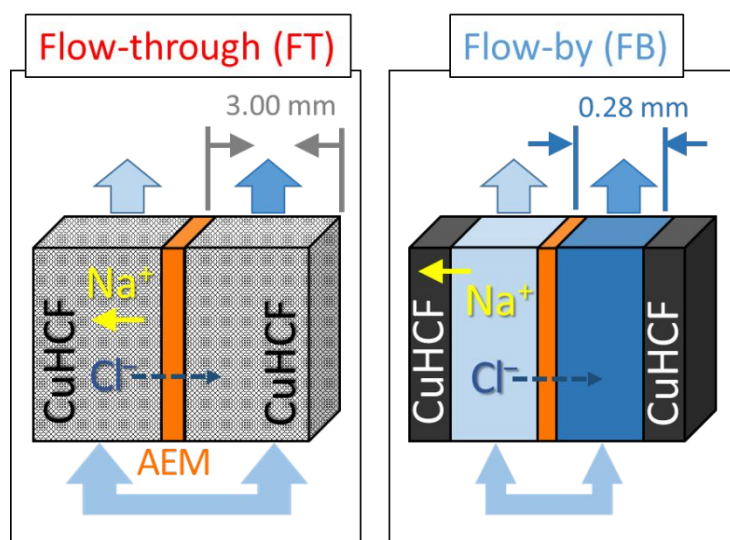
107 where  $W_w$  (g) is the weight of the electrode after it filled with water by pulling water into it using  
108 a vacuum pump,  $W_d$  (g) is the dry electrode weight (g),  $E_a$  (cm<sup>2</sup>) is the electrode surface area, and  
109  $h$  (cm) is the electrode thickness.

110 Cyclic voltammetry (CV) of each electrode was measured using a 3-electrode cell (~2 cm  
111 long by ~3 cm in diameter) containing working and counter CuHCF electrodes, and a Ag/AgCl  
112 reference electrode, at a scan rate of 1 mV s<sup>-1</sup> using 1 M NaCl.

113 **BDI Cell Construction.** The BDI cell of cylindrical chambers (30 mm exposed diameter, 7  
114 cm<sup>2</sup> effective area) containing two CuHCF electrodes separated by an AEM (106 ± 1 μm thick  
115 with an ion exchange capacity of 1.85 mmol g<sup>-1</sup>,<sup>35, 36</sup> Selemion AMV, Asahi Glass) (Figure 1).  
116 For both FT and FB operation, the water entered the bottom of the chamber and exited through  
117 the top of each chamber. In FT mode, the water flowed through the electrode that completely  
118 filled the chamber (no spacer), with flow into the other chamber blocked by the AEM. In FB  
119 mode, the same configuration was used except the water flowed through over the electrode  
120 through a fabric spacer (0.28 mm thick and 33% porosity; Sefar Nitex, 06-210/33). Rubber

121 gaskets were placed between each component in order to prevent leakage of solution and  
 122 graphite foil was used as the current collector for the CuHCF electrodes. Conductivity of the  
 123 effluent solutions was monitored using a flow-through conductivity meter (ET908, eDAQ,  
 124 Australia). Prior to desalination tests, the potentials of the two CuHCF electrodes were adjusted  
 125 to 0.4 and 1.0 V (versus Ag/AgCl reference electrodes) using a separate 3-electrode cell  
 126 containing working (CuHCF), counter (activated carbon), reference electrodes (Ag/AgCl in 3 M  
 127 NaCl), and 1 M NaCl solution prior to the desalination tests, as previously described.<sup>19</sup>

128



129

130 **Figure. 1** Schematic of flow-through (FT) and flow-by (FB) deionization cells using battery  
 131 electrodes, copper hexacyanoferrate (CuHCF), in two channels divided by an anion exchange  
 132 membrane (AEM).  
 133

134 **Desalination Experiments.** Electrochemical removal of sodium ions by the CuHCF can be

135 expressed as



136 where  $\text{Na}^+$  stands for sodium ion present in the feed solution. The CuHCF electrode can hold  
 137 sodium (3.6 Å hydrated radius) or other ions when they are similar in size to the interstitial sites

138 (3.2~4.6 Å).<sup>37-41</sup> Synthetic brackish water (50 mM NaCl) was continuously fed to the BDI cell at  
 139 a flow rate of 0.5 mL min<sup>-1</sup>, except as noted. A set current of 10 A m<sup>-2</sup> was applied at a voltage  
 140 window of ± 0.6 V using a potentiostat (VMP3, Bio-Logic), except as indicated. The NaCl  
 141 concentrations in the effluent were reported based on the measured solution conductivities.

142 Specific adsorption capacity (*SAC*, mg of Na<sup>+</sup> per gram of electrode, mg g<sup>-1</sup>) was calculated  
 143 as

$$SAC = \frac{M_{Na} \int_0^{T_c} C_{Na} dt}{E_{Mass}} \quad (3)$$

144 where  $T_c$  is the charging time or the cycling time,  $C_{Na}$  is the moles of Na<sup>+</sup> removed,  $M_{Na}$  is the  
 145 molecular weight of Na<sup>+</sup>, and  $E_{Mass}$  is the electrode mass. Specific capacity (*SC*, mAh g<sup>-1</sup>) was  
 146 calculated as

$$SC = \frac{\int_0^{T_c} I dt}{E_{Mass}} \quad (4)$$

147 where  $I$  is the applied current. Charge efficiency ( $\Lambda$ ; %) was calculated as

$$\Lambda = \frac{F \int_0^{T_c} C_{Na} dt}{\int_0^{T_c} I dt} \times 100 \quad (5)$$

148 where  $F$  is Faraday's constant (96,485 C mol<sup>-1</sup>). Cycling efficiency (*CE*; %) was calculated as

$$CE = \frac{\sum T_D}{\sum T_C} \times 100 \quad (6)$$

149 where  $T_D$  is the discharge time. The discharge and charge times are the time taken for the voltage  
 150 to increase from -0.6 to 0.6 V or decrease from 0.6 to -0.6 V at a constant current, 10 A m<sup>-2</sup>.

151 **Thermodynamic Energy Efficiency.** Energy consumption ( $E_C$ , kWh m<sup>-3</sup>) and recovery ( $E_R$ ,  
 152 kWh m<sup>-3</sup>) were calculated as<sup>19</sup>



$$E_C = \frac{\int_0^{T_s} V I T dt}{J_w} \quad (7)$$

$$E_R = \frac{\int_0^{T_f} V I T dt}{J_w} \quad (8)$$

153 where  $T_f$  is the beginning of the first half-cycle when the flows are switched ( $-0.6$  to  $0$  V when  
 154  $10 \text{ A m}^{-2}$  is applied or  $0.6$  to  $0$  V when  $-10 \text{ A m}^{-2}$  is applied),  $T_s$  is the rest of the half-cycle until  
 155 the direction of applying current is switched, and  $J_w$  is the water flux during operation (during  $T_f$   
 156 and  $T_s$ ). During the ion adsorption step ( $T_s$ ), the voltage ( $V$ ) and the current ( $I$ ) have the same  
 157 sign (either positive or negative), meaning that this step costs energy. However, during the ion  
 158 desorption step ( $T_f$ ), the voltage ( $V$ ) and the current ( $I$ ) have the different signs since ions are  
 159 released spontaneously, so that this step recovers energy. Thus, energy recovery was calculated  
 160 when the direction of the applied current is switched until the cell voltage reached  $0$  V (Figure  
 161 S1).

162 The thermodynamic energy efficiency ( $TEE$ , %) was calculated as

$$TEE = \frac{\Delta g}{E_C - E_R} \times 100 \quad (9)$$

163 The specific Gibbs free energy of separation,  $\Delta g$  ( $\text{kWh m}^{-3}$ ), was calculated as<sup>42</sup>

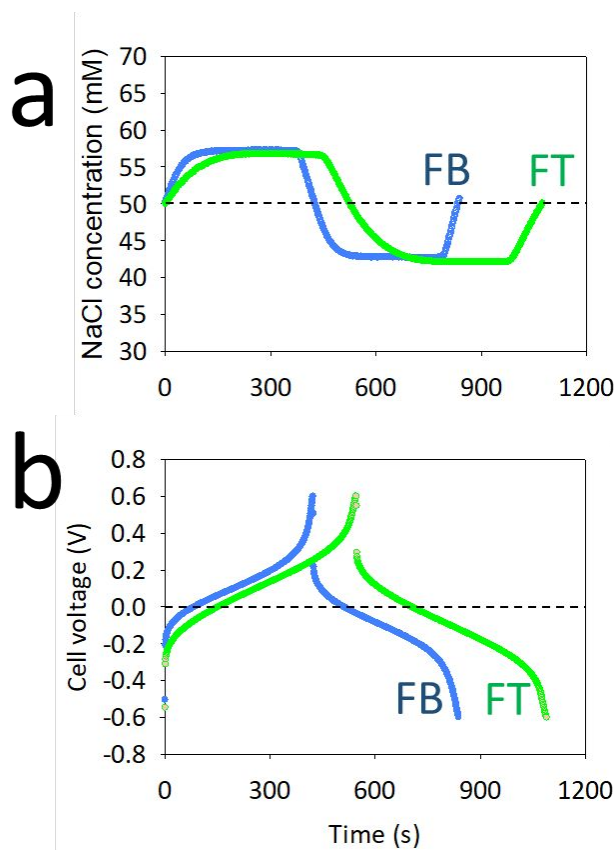
$$\Delta g = 2RT_a \left\{ \frac{C_0}{\gamma} \ln \left[ \frac{C_0 - \gamma C_D}{C_0(1 - \gamma)} \right] - C_D \ln \left[ \frac{C_0 - \gamma C_D}{C_D(1 - \gamma)} \right] \right\} \quad (10)$$

164 where  $R$  is the ideal gas constant,  $T_a$  is the absolute temperature,  $C_0$  is the feed concentration,  $C_D$   
 165 is the stabilized product water concentration, and  $\gamma$  is the water recovery. In all experiments, the  
 166 flow rate of both chambers remained the same, so the water recovery was fixed at  $50\%$  ( $\gamma = 0.5$ ).

167

## 168 Results & Discussion

169        **Flow-through vs. Flow-by Battery Electrode Performance.** The FT battery electrode  
170 could be operated for a longer period of time (18 min vs. 14 min for the FB electrode) before ion  
171 saturation occurred, resulting in a slower increase in cell voltage compared to that obtained with  
172 the FB electrode for a complete charging/discharging cycle (constant current of  $10 \text{ A m}^{-2}$ ,  
173 voltage window of  $\pm 0.6 \text{ V}$ ) (Figure 2). This longer operation time of the FT electrode can be  
174 explained by the lower ohmic (or IR) drop. When the direction of the current is changed under  
175 constant current conditions, the voltage of the electrode instantaneously decreases due to the  
176 internal resistance of the cell.<sup>43</sup> The magnitude of the change in the voltage change reflects the  
177 internal resistance of a cell, and therefore the smaller voltage drop for the FT electrode (0.3 V in  
178 2 s) shows that it had a lower internal resistance than the FB electrode (0.4 V in 2 s). This lower  
179 internal resistance was due to better dispersion of CuHCF, a longer retention time of the feed  
180 solution, and less solution resistance due to the lack of a gap between the electrode and AEM in  
181 the FT configuration compared to the FB configuration. Since both FT and FB electrodes were  
182 tested in essentially the same flow-cell architecture with the same electrode material, the  
183 influence of other factors that determine overall resistance in the electrochemical processes can  
184 be excluded in our comparisons, such as contact resistances at current collectors and collector  
185 resistance.<sup>32</sup>

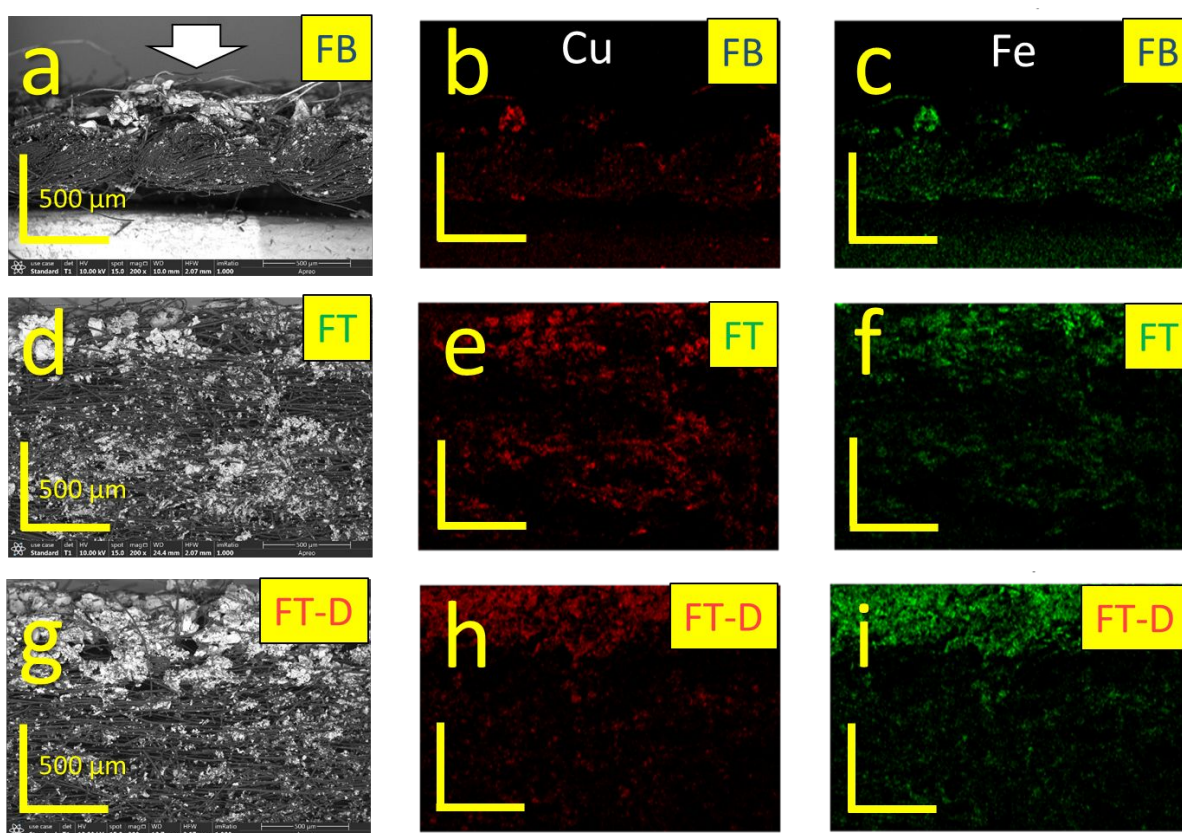


186  
187 **Figure. 2** (a) Representative effluent concentration profiles and (b) cell voltages of the FT and  
188 FB electrodes for one complete cycle. A constant current of  $10 \text{ A m}^{-2}$  was applied at a voltage  
189 window of  $\pm 0.6 \text{ V}$ .  
190

191 Although the same amount of the CuHCF ( $4 \text{ mg cm}^{-2}$ ) was used for both the FT and FB  
192 electrodes, the electrode material was better dispersed throughout the FT electrode compared to  
193 FB electrode (Figures 3 and S2). This better dispersion of the CuHCF within the electrode  
194 provided more active sites, contributing to the lower ohmic drop for the FT electrode. The longer  
195 retention time of the fluid is also known from previous studies to help reduce the ohmic drop.<sup>9</sup>  
196 Based on the thickness and porosity of the porous substrate ( $3.00 \text{ mm}$  and  $89 \pm 4\%$ ) and spacer  
197 ( $0.28 \text{ mm}$  and  $33\%$ ), the hydraulic retention time (HRT) of FT cell ( $3.74 \text{ min}$ ) was 28 times  
198 greater than FB cell ( $0.13 \text{ min}$ ). This longer HRT can also explain the slightly slower salt  
199 adsorption kinetics of the FT electrode compared to the FB electrode when the current was

200 switched. As a result of the larger HRT of the FT cells, the NaCl concentration of the effluent  
 201 solution reached a plateau more slowly when the voltage was applied compared to the FB cell  
 202 (Figure 2a). Thus, the lower internal resistance of the FT cell was most likely from its better  
 203 dispersion of CuHCF, longer HRT, and less solution resistance since the chemical composition  
 204 of the electrode itself (CuHCF and carbon-based substrate) was not changed.

205



206

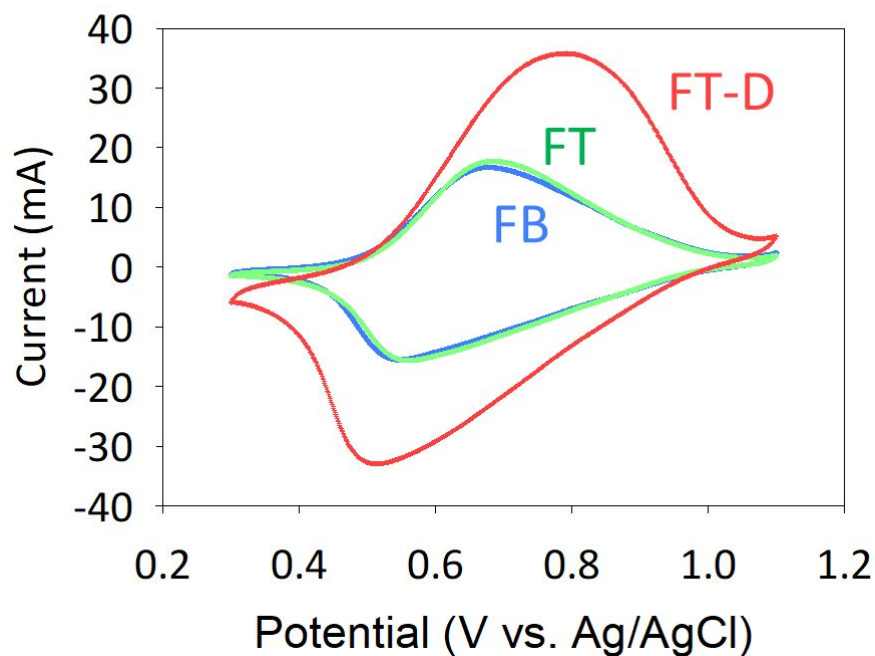
207 **Figure. 3** Cross-sectional images of the FB, FT, and FT-D (FT electrode with double CuHCF  
 208 loading) electrodes using (a, d, and g) SEM, and (b, e, and h) Cu and (c, f, and i) Fe using SEM-  
 209 EDS. The white arrow indicates the direction the slurry containing CuHCF was deposited. Scale  
 210 bars (yellow) are 500  $\mu\text{m}$  in both horizontal (x) and vertical (y) directions.

211

212 The FT electrode had a higher specific capacity ( $SC=35 \text{ mAh g}^{-1}$ ) and salt adsorption  
 213 capacity ( $SAC=19 \text{ mg-Na g}^{-1}$ ) than the FB electrode ( $SC=29 \text{ mAh g}^{-1}$ ,  $SAC=17 \text{ mg-Na g}^{-1}$ ).

214 These larger values for the FT electrode, with the same CuHCF loading, was likely due to the  
215 greater availability of active sites since both the FT and FB electrodes had the same total  
216 capacitance, as shown in the CV profiles (Figure 4). This improved performance for the FT  
217 electrode is consistent with previous findings that using three-dimensional electrodes improves  
218 electrode performances due to a large surface area and greater charge transport.<sup>44</sup> The cycling  
219 efficiencies of the two battery electrodes was both very high (100% for FT; 99% for FB),  
220 indicating nearly identical times for charging and discharging for each electrode.

221



222

223 **Figure. 4** Representative cyclic voltammetry (CV) scans of FB (blue line), FT (green line), and  
224 FT-D (red line) electrodes in a 3-electrode cell (1 M NaCl, scan rate = 1 mV s<sup>-1</sup>). The FB and FT  
225 lines overlap each other and thus are difficult to distinguish.

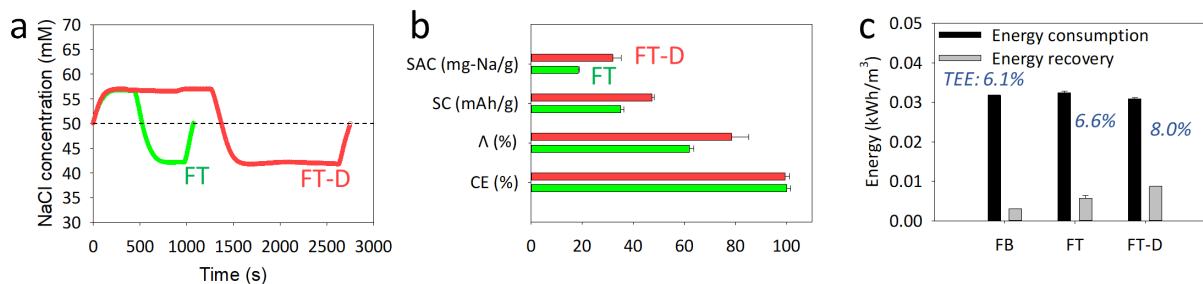
226

227 An additional experiment was conducted with a plain carbon electrode, typically used for  
228 CDI, in order to confirm that ion adsorption was not affected by the electrode capacitance. When  
229 a plain carbon cloth electrode (4 mg cm<sup>-2</sup> of activated-carbon, no CuHCF) was used, no

230 appreciable change in the effluent solution was found under the same experiment conditions as  
231 that tested for the BDI electrodes ( $10 \text{ A m}^{-2}$  and  $\pm 0.6 \text{ V}$ ) (Figure S3). Therefore, sodium ions  
232 were removed through intercalation in the presence of CuHCF and not double layer adsorption  
233 by the capacitance of the electrode.

234 **Effect of Adding More CuHCF.** Additional CuHCF was added to the graphite felt, with a  
235 maximum amount limited to  $8 \text{ mg cm}^{-2}$  of CuHCF, or double that used in the previous  
236 experiments. The FT-D electrode operation time was almost three times longer than that of the  
237 FT electrode (Figure 5a), enabling three times more desalinated water to be produced per half-  
238 cycle of operation. The FT-D electrode also had considerably greater salt adsorption ( $SAC = 32$   
239  $\text{mg-Na g}^{-1}$ ) and specific ( $SC = 47 \text{ mAh g}^{-1}$ ) capacities, and a larger charge efficiency ( $A = 78\%$ )  
240 than the FT electrodes (Figure 5b). Although the FT-D electrode had a higher capacitance than  
241 the FT electrode (Figure 4), the improved performance was mostly due to the greater mass of  
242 CuHCF, as shown by the nearly doubled salt adsorption capacity of the FT-D electrode. The  
243 CuHCF was better distributed into the whole felt FT-D electrode, compared to tests with less  
244 material (Figure 3g–i). This better CuHCF dispersion of the FT-D electrode along the substrate  
245 depth was clearly shown in the wide cross-sectional SEM image (Fig. S2). The dispersion of the  
246 CuHCF was important because higher desalination performances would not have been achieved  
247 with more CuHCF mass loading if it was not well dispersed. The cycling efficiency of the FT-D  
248 electrode remained very high ( $CE = 99\%$ ), indicating the time to charge the electrode was the  
249 same as that needed to discharge the electrode. This double loading of CuHCF could not be  
250 successfully used for the cloth electrode for the FB tests. When this amount of material was  
251 added to the FB electrode, the deposited material had an uneven surface (Figure S4c), and  
252 preliminary tests showed reduced performance (data not shown).

253



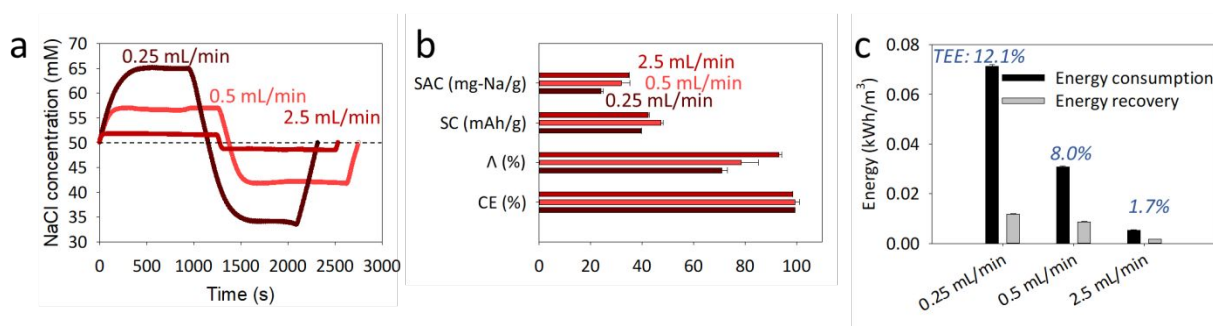
254

255 **Figure 5** (a) Representative effluent concentration profiles of FT and FT-D (FT electrode with  
 256 double loading of CuHCF) electrodes. (b) Specific adsorption capacity (*SAC*), specific capacity  
 257 (*SC*), charge efficiency (*A*), and cycling efficiency (*CE*) of the electrodes. (c) Energy  
 258 consumption and recovery, and thermodynamic energy efficiency (*TEE*) of the electrodes. A  
 259 constant current of  $10 \text{ A m}^{-2}$  was applied at a voltage window of  $\pm 0.6 \text{ V}$ . Error bars show the  
 260 range from at least duplicated experiments.  
 261

262 The FT-D electrode had an increased *TEE* of 8.0% as a result of having three times greater  
 263 energy recovery ( $0.009 \text{ kWh m}^{-3}$ ) than the FB electrode ( $0.003 \text{ kWh m}^{-3}$ ) (Figure 5c). Although  
 264 both electrodes consumed the same total amount of energy ( $\sim 0.03 \text{ kWh m}^{-3}$ ) to desalinate the  
 265 solution (50 mM to 42 mM), the total time measured during the energy recovery step using the  
 266 FT-D electrode was almost 8 times longer ( $\sim 8 \text{ min}$ ) compared to that of the FB electrode ( $\sim 1$   
 267 min). This additional time was due to the lower internal resistance, and not differences in  
 268 hydraulic retention times in the chamber, based on comparisons of the ohmic drop after the  
 269 cutoff voltage was reached. The ohmic drop was 0.2 V for the FT-D electrode, compared to 0.3  
 270 V for the FT electrode, and 0.4 V for the FB electrode (Figure S5). The energy recovery of the  
 271 FT-D electrode was also increased due to the slower rate of the voltage change of the FT-D  
 272 electrode during the overall energy recovery step than that of the FB electrode (Figure S5).

273 **Effect of Flow Rate.** The water feed was set at a faster ( $2.5 \text{ mL min}^{-1}$ ) and slower ( $0.25 \text{ mL}$   
 274  $\text{min}^{-1}$ ) flow rate to examine the impact of flow rate relative to that used in the previous tests ( $0.5$   
 275  $\text{mL min}^{-1}$ ) (Figure 6). Decreasing the flow rate to  $0.25 \text{ mL min}^{-1}$  increased salt removal

276 producing an effluent salt concentration of 34 mM, while increasing it to 2.5 mL min<sup>-1</sup>  
 277 substantially decreased salt removal, producing an effluent salt concentration of 48.5 mM  
 278 (Figure 6a). Therefore, the extent of desalination was inversely proportional to the flow rate.  
 279 However, the salt adsorption capacity and charge efficiency both increased with flow rate, with a  
 280 44% increase in *SAC* to 35 mg-Na g<sup>-1</sup> and a change in the *A* from 71% to 93% at the highest  
 281 flow rate (Figure 6b). These increases in *SAC* and *A* were due to the increased total amount of  
 282 moles of Na<sup>+</sup> ions removed at the higher flow rate, but a lower extent of ion removal relative to  
 283 the 10 times higher flow rate into the cell.  
 284



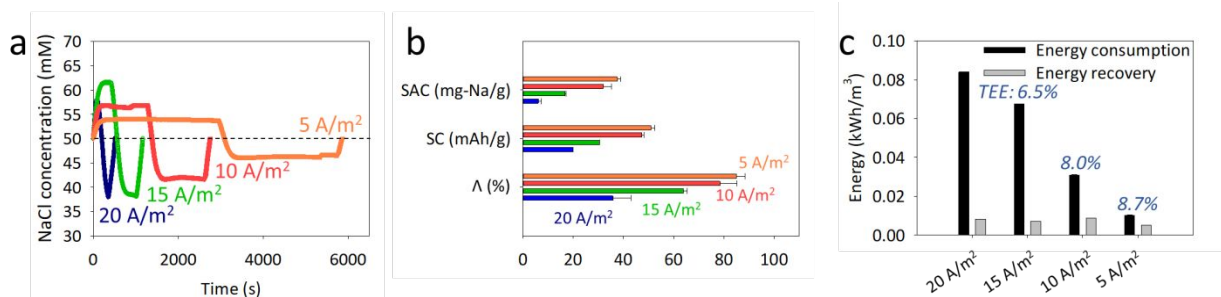
285 **Figure 6** (a) Representative effluent concentration profiles as a function of flow rate, 0.25, 0.5,  
 286 and 2.5 mL min<sup>-1</sup>, using FT-D electrodes. (b) Specific adsorption capacity (*SAC*), specific  
 287 capacity (*SC*), charge efficiency (*A*), and cycling efficiency (*CE*) at different flow rates. (c)  
 288 Energy consumption and recovery, and thermodynamic energy efficiency (*TEE*) at different flow  
 289 rates. A set current of 10 A m<sup>-2</sup> was applied at a voltage window of ± 0.6 V. Error bars show the  
 290 range from at least duplicated experiments.  
 291  
 292

293 The *TEE* increased to 12.1% by using the slower flow rate of 0.25 mL min<sup>-1</sup>, due primarily to  
 294 the greater extent of desalination (Figure 6c). At the slowest flow rate, the energy consumed was  
 295 0.071 kWh m<sup>-3</sup>, compared to 0.005 kWh m<sup>-3</sup> for the highest flow rate. Although the energy used  
 296 by the highest flow rate was only 7% of that of the slowest flow rate, the energy for desalinating  
 297 50 mM influent water to 48.5 mM was < 1% of the energy to obtain 34 mM effluent as a final  
 298 concentration. This is in an excellent agreement with literature that the higher *TEE* can be



299 obtained when the higher Gibbs free energy per volume of product water ( $\sim\Delta C$ ) was used.<sup>33, 45</sup>

300 **Effect of Current Density.** The applied current density was increased (20 and 15 A m<sup>-2</sup>) or  
 301 decreased (5 A m<sup>-2</sup>) to examine the impact of current density compared to that used in the  
 302 previous tests (10 A m<sup>-2</sup>) (Figure 7). The extent of desalination was highly dependent on the  
 303 applied current density since the Na<sup>+</sup> removal rate is dependent on the current density. Thus,  
 304 decreasing the current density produced lower effluent salt concentrations of 42 mM (10 A m<sup>-2</sup>)  
 305 and 46 mM (5 A m<sup>-2</sup>) (Figure 7a). While increasing the current density to 15 A m<sup>-2</sup> decreased  
 306 the effluent salt concentration to 38.1 mM, but no further decrease in the effluent concentration  
 307 was obtained at the highest applied current density of 20 A m<sup>-2</sup>. At the two lowest current  
 308 densities the effluent concentration was stable for a period of time. However, at the two highest  
 309 current densities, a very brief plateau (15 A m<sup>-2</sup>) or only a maximum (20 A m<sup>-2</sup>) with no plateau  
 310 was observed for the effluent salt concentration (Figure 7a). This lack of a stable plateau  
 311 indicated that the flux of Na<sup>+</sup> ions to the electrode was too low to maintain ion removal at current  
 312 densities  $\geq 15$  A m<sup>-2</sup> (Figure 7b). Thus, lower current densities are needed to maintain stable salt  
 313 removals in order to obtain high *SAC*, *SC*, and *A*.



314 **Figure 7** (a) Representative effluent concentration profiles as a function of constant current, 5,  
 315 10, 15, and 20 A m<sup>-2</sup>, using FT-D electrodes. (b) Specific adsorption capacity (*SAC*), specific  
 316 capacity (*SC*), and charge efficiency (*A*) at different constant currents. (c) Energy consumption  
 317 and recovery, and thermodynamic energy efficiency (*TEE*) at different constant currents. Error  
 318 bars show the range from at least duplicated experiments.

320

321 Decreasing the current density increased the specific adsorption capacity, specific capacity,  
322 and charge efficiency, indicating that ion removal was not limited by diffusion at the lower  
323 current densities (Figure 7b). For example, at the lowest current density ( $5 \text{ A m}^{-2}$ ), the specific  
324 adsorption capacity was more than 6 times higher ( $SAC=37 \text{ mg-Na g}^{-1}$ ), and the charge  
325 efficiency more than 2 times higher ( $A=85\%$ ) than those values obtained at  $20 \text{ A m}^{-2}$  ( $SAC=6$   
326  $\text{mg-Na g}^{-1}$ ,  $A=36\%$ ).

327 Lowering the current density decreased energy consumption (from  $0.084$  to  $0.010 \text{ kWh m}^{-3}$ ),  
328 but energy recovery was less impacted (from  $0.008$  to  $0.005 \text{ kWh m}^{-3}$ ) (Figure 7c). Thus, only  
329 10% of energy was recovered when the current density of  $20 \text{ A m}^{-2}$  was used, while 51% of  
330 energy was recovered when  $5 \text{ A m}^{-2}$  was used. Therefore, the highest  $TEE$  of 8.7% was found at  
331 a current density of  $5 \text{ A m}^{-2}$ . Unlike the set of experiments by changing the flow rate (Figure 6),  
332 decreasing current density (Figure 7) exhibited an inverse correlation between the Gibbs free  
333 energy per volume of product water ( $\sim\Delta C$ ) and  $TEE$  due to the substantial decrease of charge  
334 efficiency at the high applied current density. Based on these changes in specific adsorption  
335 capacity, specific capacity, charge efficiency, and  $TEE$  with current density, operation at  $\leq 10 \text{ A}$   
336  $\text{m}^{-2}$  appeared to provide the best balance in overall system performance.

337 **Outlook.** The use of the FT type electrodes in the BDI increased water desalination  
338 performances ( $TEE$  of  $>8.0\%$ ) due a reduction in the ohmic drop. The improved  $TEE$  is in  
339 contrast with results reported in the CDI literature that FT electrodes are less energy-efficient due  
340 to the additional resistance of the separator and the increased rate of side reactions.<sup>13, 32, 33</sup> Unlike  
341 CDI systems, the absence of a separator in the water path, the use of a relatively low applied  
342 voltage, and the lower internal resistance in the BDI system all combine to increase  $TEE$  values  
343 from  $\sim 6\%$  to 8%. The energy losses due to the higher pressures needed to force the liquid

344 through the felt substrate were not included in this calculation. One way to further improve  
345 performance, and reduce the energy needed to pump water through the electrode is to reduce the  
346 CuHCF particle size. The particles used here were  $\sim 200\ \mu\text{m}$  in size (Figure S2), which could  
347 have clogged some of the pores in the felt. A reduction in electrode permeability was previously  
348 shown to reduce the salt adsorption rate of the process.<sup>23</sup> Therefore, it might be possible to  
349 further improve the *TEE* and reduce energy needed for pumping by loading smaller particles  
350 onto the electrode fibers. However, flow through a porous bed of these particles alone, rather  
351 than primarily through the fibers, would increase pumping energy as the permeability changes  
352 inversely with particle size.

353 The optimal operation of the BDI systems depends on a number of factors, including flow  
354 rate, current density, and flow path. While lowering the flow rate improves the *TEE*, the extent of  
355 desalination is also reduced, offsetting this improvement. Increasing the current density also  
356 would further decrease the *TEE*. A more practical approach to improve energy efficiency would  
357 be to use 2–3 pairs of ion exchange membranes to desalinate additional water as previously  
358 shown.<sup>19</sup> Another issue that affects performance is the flow path through the electrode. The flow  
359 through the porous electrode used here may not be uniform, so a more channelized flow  
360 arrangement could improve performance. For example, in a recent study, a serpentine flow path  
361 was used to better direct the flow across all of the intercalation material used on the electrode.<sup>23</sup>  
362 Ultimately, if a BDI system using an FT electrode can achieve a higher *TEE* over other processes  
363 in brackish water desalination, the electrochemical-based desalination system will have an  
364 advantage not only in terms of energy consumption but also due to an improved energy  
365 efficiency.

366

367 ■ **ASSOCIATED CONTENT**

368 **Supporting Information**

369 Details on the effluent and cell voltage profiles recorded by using a FB electrode, the surface and  
370 cross-sectional SEM images of the FB, FT, and FT-D electrodes, the concentration profiles of  
371 NaCl effluent using activated carbon electrodes, the photographs of the electrodes, and the cell  
372 voltage profiles recorded by using the FB, FT, and FT-D electrodes during the energy recovery  
373 step.

374

375 ■ **AUTHOR INFORMATION**

376 **Corresponding Author**

377 \*(B.E.L.) E-mail [blogan@psu.edu](mailto:blogan@psu.edu); Ph +1-814-863-7908; Fax +1 814 863-7304.

378 **ORCID**

379 Moon Son: 0000-0002-3770-148X

380 Wulin Yang: 0000-0003-3590-5080

381 Johannes S. Vrouwenvelder: 0000-0003-2668-2057

382 Christopher A. Gorski: 0000-0002-5363-2904

383 Bruce E. Logan: 0000-0001-7478-8070,

384 **Notes**

385 The authors declare no competing financial interest

386

387 ■ **ACKNOWLEDGMENTS**

388 This research was supported by the King Abdullah University of Science and Technology  
389 (KAUST) (OSR-2017-CPF-2907-02) and Penn State University. Support for V.P. and C.A.G.  
390 was provided by the National Science Foundation under Grant No. 1749207.

391

392

393 ■ **REFERENCES**

- 394 (1) Porada, S.; Zhao, R.; van der Wal, A.; Presser, V.; Biesheuvel, P. M., Review on the  
395 science and technology of water desalination by capacitive deionization. *Prog. Mater.*  
396 *Sci.* **2013**, *58*, (8), 1388-1442.
- 397 (2) AlMarzooqi, F. A.; Al Ghaferi, A. A.; Saadat, I.; Hilal, N., Application of capacitive  
398 deionisation in water desalination: A review. *Desalination* **2014**, *342*, 3-15.
- 399 (3) Jeon, S.-i.; Park, H.-r.; Yeo, J.-g.; Yang, S.; Cho, C. H.; Han, M. H.; Kim, D. K.,  
400 Desalination via a new membrane capacitive deionization process utilizing flow-  
401 electrodes. *Energy Environ. Sci.* **2013**, *6*, (5), 1471-1475.
- 402 (4) Lee, J.; Kim, S.; Kim, C.; Yoon, J., Hybrid capacitive deionization to enhance the  
403 desalination performance of capacitive techniques. *Energy Environ. Sci.* **2014**, *7*, (11),  
404 3683-3689.
- 405 (5) Kim, Y.; Logan, B. E., Series assembly of microbial desalination cells containing stacked  
406 electro dialysis cells for partial or complete seawater desalination. *Environ. Sci. Technol.*  
407 **2011**, *45*, (13), 5840-5845.
- 408 (6) Kim, Y.; Logan, B. E., Microbial reverse electro dialysis cells for synergistically  
409 enhanced power production. *Environ. Sci. Technol.* **2011**, *45*, (13), 5834-5839.
- 410 (7) Schlumpberger, S.; Lu, N. B.; Suss, M. E.; Bazant, M. Z., Scalable and continuous water  
411 deionization by shock electro dialysis. *Environ. Sci. Technol. Lett.* **2015**, *2*, (12), 367-372.

- 412 (8) Son, M.; Kim, T.; Yang, W.; Gorski, C. A.; Logan, B. E., Electro-forward osmosis.  
413 *Environ. Sci. Technol.* **2019**, *53*, (14), 8352-8361.
- 414 (9) Zhao, R.; Porada, S.; Biesheuvel, P. M.; van der Wal, A., Energy consumption in  
415 membrane capacitive deionization for different water recoveries and flow rates, and  
416 comparison with reverse osmosis. *Desalination* **2013**, *330*, 35-41.
- 417 (10) Zhao, R.; Biesheuvel, P. M.; van der Wal, A., Energy consumption and constant current  
418 operation in membrane capacitive deionization. *Energy Environ. Sci.* **2012**, *5*, (11), 9520-  
419 9527.
- 420 (11) Lee, J.-H.; Bae, W.-S.; Choi, J.-H., Electrode reactions and adsorption/desorption  
421 performance related to the applied potential in a capacitive deionization process.  
422 *Desalination* **2010**, *258*, (1), 159-163.
- 423 (12) Farmer, J. C.; Fix, D. V.; Mack, G. V.; Pekala, R. W.; Poco, J. F., Capacitive deionization  
424 of NaCl and NaNO<sub>3</sub> solutions with carbon aerogel electrodes. *J. Electrochem. Soc.* **1996**,  
425 *143*, (1), 159-169.
- 426 (13) Długołęcki, P.; van der Wal, A., Energy recovery in membrane capacitive deionization.  
427 *Environ. Sci. Technol.* **2013**, *47*, (9), 4904-4910.
- 428 (14) Ahualli, S.; Iglesias, G. R.; Fernández, M. M.; Jiménez, M. L.; Delgado, Á. V., Use of  
429 soft electrodes in capacitive deionization of solutions. *Environ. Sci. Technol.* **2017**, *51*,  
430 (9), 5326-5333.
- 431 (15) Zhao, R.; Biesheuvel, P.; Miedema, H.; Bruning, H.; Van der Wal, A., Charge efficiency:  
432 a functional tool to probe the double-layer structure inside of porous electrodes and  
433 application in the modeling of capacitive deionization. *J. Phys. Chem. Lett.* **2009**, *1*, (1),  
434 205-210.
- 435 (16) Zhang, C.; He, D.; Ma, J.; Tang, W.; Waite, T. D., Faradaic reactions in capacitive  
436 deionization (CDI) - problems and possibilities: A review. *Water Res.* **2018**, *128*, 314-  
437 330.
- 438 (17) Tang, W.; He, D.; Zhang, C.; Kovalsky, P.; Waite, T. D., Comparison of Faradaic  
439 reactions in capacitive deionization (CDI) and membrane capacitive deionization (MCDI)  
440 water treatment processes. *Water Res.* **2017**, *120*, 229-237.
- 441 (18) Suss, M. E.; Presser, V., Water desalination with energy storage electrode materials.  
442 *Joule* **2018**, *2*, (1), 10-15.
- 443 (19) Kim, T.; Gorski, C. A.; Logan, B. E., Low energy desalination using battery electrode  
444 deionization. *Environ. Sci. Technol. Lett.* **2017**, *4*, (10), 444-449.
- 445 (20) Byles, B. W.; Cullen, D. A.; More, K. L.; Pomerantseva, E., Tunnel structured  
446 manganese oxide nanowires as redox active electrodes for hybrid capacitive deionization.  
447 *Nano Energy* **2018**, *44*, 476-488.
- 448 (21) Kim, S.; Yoon, H.; Shin, D.; Lee, J.; Yoon, J., Electrochemical selective ion separation in  
449 capacitive deionization with sodium manganese oxide. *J. Colloid Interface Sci.* **2017**,  
450 *506*, 644-648.
- 451 (22) Tang, W.; Liang, J.; He, D.; Gong, J.; Tang, L.; Liu, Z.; Wang, D.; Zeng, G., Various cell  
452 architectures of capacitive deionization: Recent advances and future trends. *Water Res.*  
453 **2019**, *150*, 225-251.
- 454 (23) Reale, E. R.; Shrivastava, A.; Smith, K. C., Effect of conductive additives on the  
455 transport properties of porous flow-through electrodes with insulative particles and their  
456 optimization for Faradaic deionization. *Water Res.* **2019**, *165*, 114995.

- 457 (24) Kim, T.; Gorski, C. A.; Logan, B. E., Ammonium removal from domestic wastewater  
458 using selective battery electrodes. *Environ. Sci. Technol. Lett.* **2018**, *5*, (9), 578-583.
- 459 (25) Qin, M.; Deshmukh, A.; Epsztein, R.; Patel, S. K.; Owoseni, O. M.; Walker, W. S.;  
460 Elimelech, M., Comparison of energy consumption in desalination by capacitive  
461 deionization and reverse osmosis. *Desalination* **2019**, *455*, 100-114.
- 462 (26) Remillard, E. M.; Shocron, A. N.; Rahill, J.; Suss, M. E.; Vecitis, C. D., A direct  
463 comparison of flow-by and flow-through capacitive deionization. *Desalination* **2018**,  
464 *444*, 169-177.
- 465 (27) Avraham, E.; Bouhadana, Y.; Soffer, A.; Aurbach, D., Limitation of charge efficiency in  
466 capacitive deionization I. On the behavior of single activated carbon. *J. Electrochem.*  
467 *Soc.* **2009**, *156*, (6), P95-P99.
- 468 (28) Suss, M. E.; Baumann, T. F.; Bourcier, W. L.; Spadaccini, C. M.; Rose, K. A.; Santiago,  
469 J. G.; Stadermann, M., Capacitive desalination with flow-through electrodes. *Energy*  
470 *Environ. Sci.* **2012**, *5*, (11), 9511-9519.
- 471 (29) Avraham, E.; Noked, M.; Cohen, I.; Soffer, A.; Aurbach, D., The dependence of the  
472 desalination performance in capacitive deionization processes on the electrodes PZC. *J.*  
473 *Electrochem. Soc.* **2011**, *158*, (12), P168-P173.
- 474 (30) Cohen, I.; Avraham, E.; Noked, M.; Soffer, A.; Aurbach, D., Enhanced charge efficiency  
475 in capacitive deionization Achieved by surface-treated electrodes and by means of a third  
476 electrode. *J. Phys. Chem. C* **2011**, *115*, (40), 19856-19863.
- 477 (31) Zhang, C.; He, D.; Ma, J.; Tang, W.; Waite, T. D., Comparison of faradaic reactions in  
478 flow-through and flow-by capacitive deionization (CDI) systems. *Electrochim. Acta*  
479 **2019**, *299*, 727-735.
- 480 (32) Hawks, S. A.; Ramachandran, A.; Porada, S.; Campbell, P. G.; Suss, M. E.; Biesheuvel,  
481 P. M.; Santiago, J. G.; Stadermann, M., Performance metrics for the objective assessment  
482 of capacitive deionization systems. *Water Res.* **2019**, *152*, 126-137.
- 483 (33) Hemmatifar, A.; Ramachandran, A.; Liu, K.; Oyarzun, D. I.; Bazant, M. Z.; Santiago, J.  
484 G., Thermodynamics of Ion Separation by Electrosorption. *Environ. Sci. Technol.* **2018**,  
485 *52*, (17), 10196-10204.
- 486 (34) Celik, E.; Liu, L.; Choi, H., Protein fouling behavior of carbon nanotube/polyethersulfone  
487 composite membranes during water filtration. *Water Res.* **2011**, *45*, (16), 5287-5294.
- 488 (35) Geise, G. M.; Cassady, H. J.; Paul, D. R.; Logan, B. E.; Hickner, M. A., Specific ion  
489 effects on membrane potential and the permselectivity of ion exchange membranes. *Phys.*  
490 *Chem. Chem. Phys.* **2014**, *16*, (39), 21673-21681.
- 491 (36) Le, X. T.; Bui, T. H.; Viel, P.; Berthelot, T.; Palacin, S., On the structure-properties  
492 relationship of the AMV anion exchange membrane. *J. Membr. Sci.* **2009**, *340*, (1), 133-  
493 140.
- 494 (37) Geise, G. M.; Paul, D. R.; Freeman, B. D., Fundamental water and salt transport  
495 properties of polymeric materials. *Prog. Polym. Sci.* **2014**, *39*, (1), 1-42.
- 496 (38) Wessells, C. D.; Peddada, S. V.; McDowell, M. T.; Huggins, R. A.; Cui, Y., The effect of  
497 insertion species on nanostructured open framework hexacyanoferrate battery electrodes.  
498 *J. Electrochem. Soc.* **2011**, *159*, (2), A98-A103.
- 499 (39) Itaya, K.; Ataka, T.; Toshima, S., Spectroelectrochemistry and electrochemical  
500 preparation method of Prussian blue modified electrodes. *J. Am. Chem. Soc.* **1982**, *104*,  
501 (18), 4767-4772.

- 502 (40) Wang, R. Y.; Shyam, B.; Stone, K. H.; Weker, J. N.; Pasta, M.; Lee, H. W.; Toney, M.  
503 F.; Cui, Y., Reversible multivalent (monovalent, divalent, trivalent) ion insertion in open  
504 framework materials. *Adv. Energy. Mater.* **2015**, *5*, (12), 1401869.
- 505 (41) Scholz, F.; Dostal, A., The formal potentials of solid metal hexacyanometalates. *Angew*  
506 *Chem. Int. Ed. Engl.* **1996**, *34*, (23 - 24), 2685-2687.
- 507 (42) Wang, L.; Dykstra, J. E.; Lin, S., Energy Efficiency of Capacitive Deionization. *Environ.*  
508 *Sci. Technol.* **2019**, *53*, (7), 3366-3378.
- 509 (43) Zhang, D.; Yan, T.; Shi, L.; Peng, Z.; Wen, X.; Zhang, J., Enhanced capacitive  
510 deionization performance of graphene/carbon nanotube composites. *J. Mater. Chem.*  
511 **2012**, *22*, (29), 14696-14704.
- 512 (44) Wang, H.; Zhang, D.; Yan, T.; Wen, X.; Zhang, J.; Shi, L.; Zhong, Q., Three-dimensional  
513 macroporous graphene architectures as high performance electrodes for capacitive  
514 deionization. *Journal of Materials Chemistry A* **2013**, *1*, (38), 11778-11789.
- 515 (45) Lin, S., Energy Efficiency of Desalination: Fundamental Insights from Intuitive  
516 Interpretation. *Environ. Sci. Technol.* **2020**, *54*, (1), 76-84.

517

518 TOC Art

519

520

